Wasit Journal of Engineering Sciences

Journal homepage: https://ejuow.uowasit.edu.iq

Numerical Study of Sedimentation and Flow Pattern at the Open Channel Intake

Rana A. Al-Zubaidy [1], Ali N. Hilo [1]

Affiliations
1 Civil Engineering Department, Wasit University, Iraq

Correspondence
Rana A. Al-Zubaidy,
Civil Engineering Department,
Wasit University, Iraq

Email: civile913@gmail.com

Received
11-January-2022
Revised
15-March-2022
Accepted
20-April-2022

Doi: 10.31185/ejuow.Vol10.Iss3.279

Abstract

Generally, open channel lateral intake structures are extensively used in the water and environmental projects. The passing flow at side intakes is mostly turbulence containing vertical and horizontal spiral currents causing sediment problems. The flow separation region in the intake channel is critical for sediment and water distribution during the diversion. It denotes a large reduction in the possible breadth of the lateral branch's incoming flow, as well as a place where sediment has collected, obstructing the deviated flow.

This study aims to reduce and control sediment problems at the lateral intake by improving the flow pattern at this area using three-dimensional numerical models simulated in CFD, ANSYS Fluent software. The correctness of the three-dimensional numerical model was validated by a previous experimental study that showed good accuracy. Different discharge ratios and a range of shape designs were used to simulate the flow pattern at the intake channel junction. The findings demonstrated that the separation zone measurements minimize as the discharge ratio increases. Based on the changing the intake entrance shape results, cutting the outer boundary of the canal entrance widens the separation area, as well as an additional separation spot as the cutting size grows. In contrast with the internal chamfered angle models of the intake inlet, the separation area dimensions are reduced. The chamfered and rounded inner intake edge model with 30^{o} angle to the main channel flow direction and the length of the chamfered side that normal to the flow direction (c value) equal to three-quarters of the intake width was noticed to be the best design for lessening separation extent in this study. Thereby, the reduction ratio of the separation area width and length reaches in this case to 90% and 72%, respectively.

Keywords: Lateral intake, Separation zone, Fluent, Sedimentation.

الخلاصة: يتم استخدام قناة السحب المتفرعة من الأنهار والقنوات المائية في مشاريع المياه والبيئة، حيث يكون التدفق المنتقل إلى هذه القنوات الجانبية غالبا عبارة عن تدفق مضطرب يحتوي على تيارات لولبية رأسية وأفقية. هذه التيارات لها دور أساس في تفاقم مشاكل تراكم الرواسب في القنوات الجانبية. منطقة فصل التدفق هي دوامة تنشأ في مدخل القناة الجانبية لها تأثير كبير على توزيع الرواسب والمياه اثناءالتحويل؛ مما يسبب سحب الرواسب من المجرى الرئيس وترسيبها عند مدخل القناة . تراكم طبقات الرواسب عند مدخل قناة السحب الجانبية يسبب انخفاضا كبيرا في سعة تدفق الجريان المتحول إلى الفرع الجانبي؛مما يسبب ضحالة المياه وخسائرا في المنشآت التي تخدمها قناة السحب ،إضافة إلى إمكانية تغير مسار الجريان عند تراكم هذه الرواسب وعدم إزالتها مع مرور الزمن.

تهدف هذه الدراسة إلى تقليل مشاكل الرواسب والتحكم فيها عند مدخل قناة السحب الجانبية،عن طريق تحسين نمط التدفق باستخدام نماذج رقمية ثلاثية الأبعاد،حيث تمت محاكاتها بواسطة برنامجCFD, ANSYS FLUENT. تم التحقق من صحة النموذج العددي ثلاثي الأبعاد من خلال دراسة تجريبية سابقة،حيث أظهرت النتائج أن النموذج الرقمي ذو دقة عالية. بعد ذلك تم محاكاة نمط التدفق عند تقاطع القناة الجانبي، وذلك باستخدام نسب تصريف وتصاميم هندسية مختلفة. أظهرت النتائج أن ابعاد منطقة الفصل تقل مع زيادة نسبة التصريف للقناة الفرعية. بناء على نتائج نمذجة تصاميم لمختلف الخصائص الهندسية لمدخل القناة الجانبية؛فإن قطع الزاوية الخارجية لمدخل القناةالفرعية (الزاوية المقابلة لمنبع القناة الرئيسة) بزوايا معينة يوسع منطقة الفصل، بالإضافة إلى ظهور منطقة فصل إضافية،مع زيادة حجم القطع، على العكس من نماذج زاوية قناة السحب الداخلية المقطوعة بشكل مائل،

حيث تقلل حجم منطقة الفصل. تم التوصل في هذه الدراسة إلى أن نموذج قناة السحب ذا الزاوية الداخلية المقطوعة بزاوية٣٠ درجة مع إتجاه التدفق وبمسافة عمودية على اتجاه الجريان بمقدار ثلاثة أرباع عرض قناة السحب مع استدارة حافة القطع هو افضل نموذج لخفض حجم منطقة الفصل،حيث تصل نسبة انخفاض عرض وطول منطقة الفصل في هذا النموذج إلى **٩٠%** و**٧٢%** على التوالي.

1. INTRODUCTION

Lateral intake and confluence are the forms of open channel junctions (Figure 1) [1]. Several applications of environmental and hydraulic engineering like navigable watercourses, irrigation, power station facilities used in cooling or steam production, and run-of-the-river hydropower facilities use open channel intakes. Protection of these channels against erosion, sedimentation, sediment transport, and deterioration [2-4], therefore, becomes crucial. While it is known that the flow mechanic at the intake junction is complicated, and reveals non-uniform 3D flow patterns, it is still not fully understood, [5-7]. Hence, several problems arise in this region, such as asymmetric flow pattern-related energy losses and the common issue of sedimentation [5]. The accumulation of sediment most often is the reason for irrigation canals to decrease incapacity; it can also be hazardous to the mechanical parts of the water systems in power plants [8,9]. Upgrading the work in a canal system includes the principal issues of efficient sediment management, allocation of a substantial portion of the annual budget for repair and maintenance, and removal of the sediment [10]. The main objective of the engineers, therefore, is to design an intake having a high discharge of flow with low delivery of sediment [7].

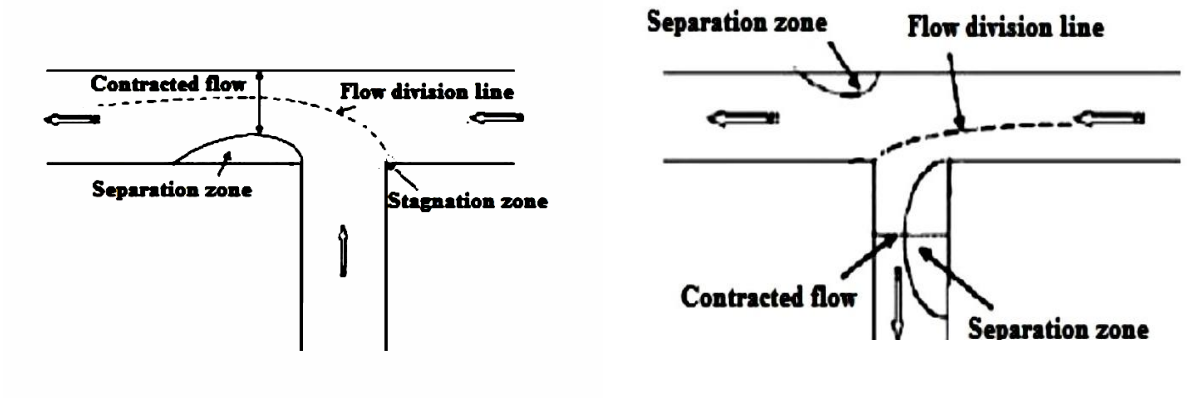

(a) (b)

Figure 1 Open channel junction types. (a) Confluence and (b) lateral intakke [1].

As the intake structures reroute some amount of the river flow, they may induce certain alterations in the hydraulic conditions at the entrance of the flow. Reversal and separation zones, streamwise currents, a reduced flow area in the branch channel, and a stagnation point at the downstream corner of the intake mouth are all common features of this flow. Also, along the length of the far wall of the main channel, just downstream of the diversion, separation may be observed, caused by an expansion in the flow. The features of the diversion flow are displayed in Figures 2 and 3 [5,8, 9,10 Bulle]. Close to the upstream intake bank, the intake channel shows a recirculation area (separation zone) near the base, having negative velocities (opposite to the flow movement). This area has been recognized to induce a substantial portion of the sediment which enters the lateral branch to be deposited (Figure 4). Upstream from the diversion, a dividing stream surface is clearly seen. This divides the flow entering the branch channel from the one which enters directly into the main channel. Characteristically, this surface reveals that the redirected region at the lateral channel is greater when it is nearer to the bed surface. Due to the least velocities presented in this place, counteracting the centrifugal forces and changing the direction of the flows in this region are easier to accomplish [11-13]. This is one of the causes for a major portion of the sediment to gain entry into the lateral branch, particularly when the sediment transportation occurs principally as a bedload [14]. It is at the stagnation point, which is formed at the upstream corner of the juncture, that the two main and sub-main flows first come into contact, and in this zone, the flow velocity is almost zero [15]. Further, as these vortices are observed to flow in a helical pattern, the morphology and shear stress of the riverbed get altered [16]. The low-shear district identified parallel to the stagnation point shows a tendency towards sedimentation. The flow velocity increases greatly at the maximum velocity zone or the contraction zone, and wherever the shear stress is higher than the critical stress, local erosion is observed [15,18,19].

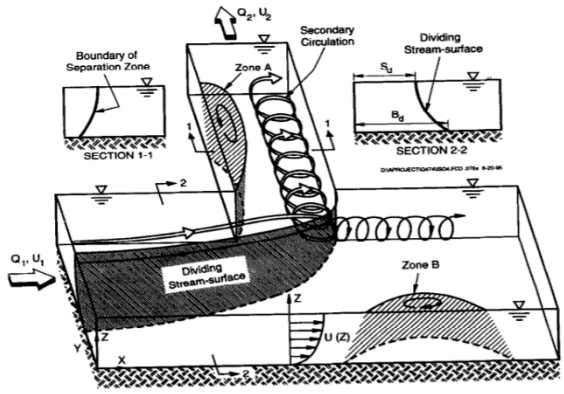

Figure 2 Formation of vertical and lateral eddies at a lateral intake [9].

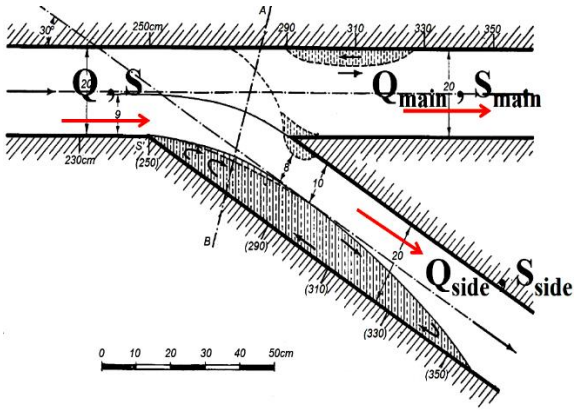

Figure 3 Representation of the experiments performed by Bulle [10]; (Q is flow discharge; S indicates sediment discharge).

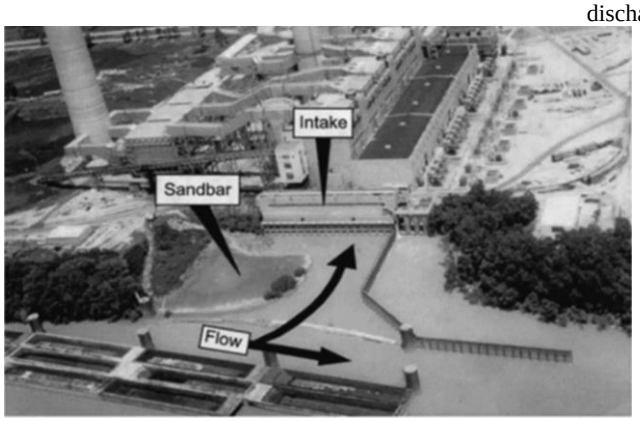

Figure 4 Sediment accumulated at the separation zone at Ohio river intake [9].

Numerous studies have been done for sediment control at the intakes, a complex problem recognized in river engineering. Prior studies have revealed sediment-related problems connected with lateral intakes [11,12-14]. Experimental observations in earlier works indicate the disproportionate propensity for sediment to enter the lateral channel, as seen in Figure 3. This phenomenon, termed the Bulle effect, is associated with the flow patterns that occur in the region of the diversion. Additionally, Several laboratory and numerical analyses have been done in the absence of sediment discharge, the aims of which were to measure and describe the flow velocity field and water surface [8, 15-17]. Karami Moghadam et al. [18] developed a physical model of the 55º angle branch channel with a rectangular section to study the impacts of the inlet form, angle, discharge ratio, and erosion, as well as the presence of submerged vanes and shear stress at the water intake. All the experiments were performed using a long rectangular flume. The significant results showed that the mouth of the intake was made with a rounded edge it induced a rise in erosion and a drop in sedimentation, thus causing a reduction in the sediments deposited. Also, as the diversion ratio rises, there is a corresponding decline in the sedimentation rate at the intake, coupled with an escalation in the degree of erosion. Helal [19] studied experimentally and numerically minimizing the effect of different shapes of the downstream junction edge (sharp, chamfer, and round) on the separation zone at an open channel confluence. Results reveal that the rounded edge minimized the separation zone width and scour depth with a reduction ratio of 47%, and 85%, respectively, compared to the model of a sharp edge. Additionally, the separation zone downstream of the junction was diminished at a rounded edge radius of 1.33 of the main channel width.

Regarding the numerical studies, the results of the three-dimensional simulation showed substantially closer concurrence with the experiments than did the two-dimensional ones because of the complexity of the flow structure [3]. In their studies, Pizardeh & Shamloo [3], Ramamurthy et al. [8], Neary et al. [9 and Rezapour et al. [20] revealed that the size of this recirculated area was dependent upon the diversion ratio (discharge ratio). When the discharge ratios were higher (increased water flow into the side-channel) there is narrowing and shortening of the recirculation area. These dimensions are also affected by the intake angle, which reduces when the angle decreases. This is caused by the smoother entry of the water into the lateral branch [17]. Concerning the variations that these dimensions reveal with depth, a few theoretical studies for flow characteristics at the diversion open channel were advanced over the years. Ramamurthy et al. [21] proposed an equation to describe the discharge ratio in terms of the inlet Froude number and the depth ratio of the main channel, before and after the diversion. Furthermore, Lama et

al. [22] used the mass and momentum conservation formulae across a specific control volume to produce a formula for the diversion discharge under a range of flow circumstances for the flow into the side channel.

From the literature review done, the Bulle Effect continues to be investigated from 1926 onwards, the time of its advent. The complex 3D flow patterns and hydrodynamics alone (excluding the sediments) in the branch or lateral channel are also not wholly understood to date, probably because traditional laboratory experiments involve physical limitations. Over the recent decades, the technological advancements and use of computer models, particularly in Computational Fluid Dynamics (CFD) of late, have opened up avenues for more intense numerical examination of this occurrence in the bifurcating open channel flows. For a better understanding and measurement of the complexity of the diversion flow demeanor, numerical calculations are used.

This study aims to reduce the sediment-related problems at the lateral intake channel. Using ANSYS Fluent CFD software, numerical analyses revealed the streamlines with variations in the velocity magnitudes, wall shear stresses, and flow vortex measurements were investigated and improved. The effects exerted by the different discharge ratios and changes in the shape of the intake entrance on the flow pattern in the intake and the influence on sediment concerns are explored.

2. NUMERICAL SIMULATION

Computational Fluid Dynamics (CFD) is being increasingly used to model fluid flow and heat transport. Today, CFD is frequently used in a wide range of sophisticated applications. This method reduces the expenditure involved in physical experimentations, especially as the computer speeds up the processes. In fact, CFD enables the prediction of the results even prior to doing the tests and even helps to set up the experiments more efficiently. The commercial codes show greater efficiency and appeal when employed to simulate the events in a wide range of engineering applications. The mathematical formulation in physical problems includes a series of Partial Differential Equations (PDE) that required numerical solving, following the Finite Volume Method (FVM). In this paper, the governing equations are solved with the use of the commercial CFD package ANSYS [23]. The 3D turbulent flows of the lateral channel properties were examined in this study for the separate cases, using the commercial software ANSYS FLUENT, version 19.2.

2.1. Governing equations

In open channels, the governing equations for the flow include the incompressible and Reynolds Averaged Navier–Stokes (RANS) equations. In the ANSYS FLUENT simulation algorithms, the equations of continuity and momentum were applied for incompressible flows [24].

In the Newtonian fluid flow of volumetric mass ρ, the equations mentioned were employed for a specific control volume. The continuity and momentum equations in the Cartesian x, y, and z coordinates are expressed as given:

Continuity equation:

$$\frac{\partial \rho}{\partial t} + \nabla \cdot (\rho V) = 0 \tag{1}$$

Momentum equations:

$$\frac{\partial (\rho u)}{\partial t} + \nabla \cdot (\rho u V) = -\frac{\partial p}{\partial x} + \frac{\partial \tau_{xx}}{\partial x} + \frac{\partial \tau_{yx}}{\partial y} + \frac{\partial \tau_{zx}}{\partial z} + \rho f_x \tag{2}$$

$$\frac{\partial (\rho v)}{\partial t} + \nabla \cdot (\rho v V) = -\frac{\partial p}{\partial y} + \frac{\partial \tau_{xy}}{\partial x} + \frac{\partial \tau_{yy}}{\partial y} + \frac{\partial \tau_{zy}}{\partial z} + \rho f_y \tag{3}$$

$$\frac{\partial (\rho w)}{\partial t} + \nabla \cdot (\rho w V) = -\frac{\partial p}{\partial z} + \frac{\partial \tau_{xz}}{\partial x} + \frac{\partial \tau_{yz}}{\partial y} + \frac{\partial \tau_{zz}}{\partial z} + \rho f_z \tag{4}$$

Where t indicates time, ρ implies the density, f represents the body forces on the fluid element, τ is the stress tensor (viscous stresses), and p denotes pressure. The velocity component (V) and the vector operator for the Cartesian coordinates (∇) are computed as:

$$V = ui + vj + wk \tag{5}$$

$$\nabla \equiv i\frac{\partial}{\partial x} + j\frac{\partial}{\partial y} + k\frac{\partial}{\partial z} \tag{6}$$

Where i, j and k are the unit vectors of the *x*, *y*, and *z* axes, respectively.

2.2. Validation

The laboratory findings of Omidbeigi et al. [25], was appointed to study the numerical model of the flow in the lateral intake. Omidbegi et al. [25] conducted experimental and numerical investigations of the three-dimensional flow properties at the diversion channel. From the results, it is evident that the recirculating region width at the intake channel decreases by boosting the discharge ratio. On investigating the flow attitude at the intake entrance, it was found that a secondary flow is created at the diversion port. As the discharge ratio rises, these secondary currents get stronger. Consequently, greater sediment bedload inflow the diversion channel. All the experiments were performed in the 90 ° diversion channels. While the main channel is 18 m in length, the branch channel was 3m in length, and in both the main and intake channels the flow depth is 15 cm. The main and intake channels are 1m and 0.4 m wide, respectively. A diversion channel was introduced at a distance of 11.43 m from the channel beginning. A rigid-bed environment was selected for the experiment, as revealed in Figure 5, with a constant inlet flow discharge of 58 liter/sec. In this work, the flow parameters used in the modeling are similar to the ones adopted in the laboratory test.

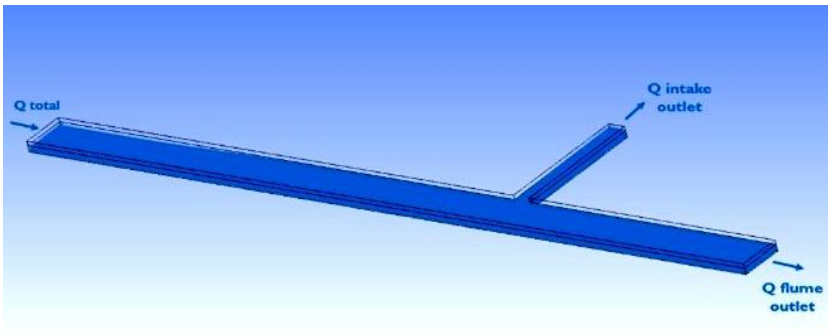

(a)

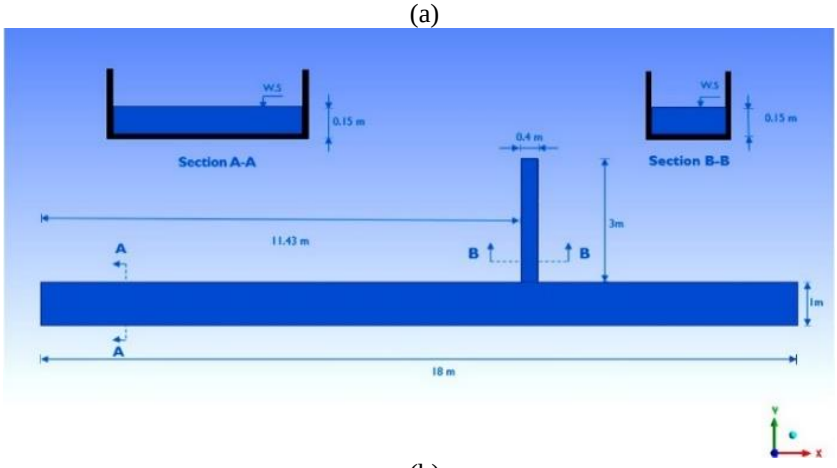

(b)

Figure 5 Laboratory flume setup of Omidbeigi et al. [25]. (a) A view of the experimental channel. (b) Top view of the flume.

*2.2.1.*Geometry and meshing

The pre-processor ANSYS DesignModeler and ANSYS Meshing programs enable the creation of the three-dimensional geometry and mesh generation of the problem (Figure 6). For the whole domain, tetrahedral items are employed in the simulation. The grid is highly concentrated and near the edge and curves so that the numerical simulations are accurate; another reason is that both the grid size and computational time can be saved by utilizing the options of capture curvature and proximity provided in the meshing solver.

The mesh metric values assessed using the ANSYS meshing solver were applied to check the mesh quality, which was endorsed by the favorite limits of these factors as cited in Table 1 [26-28]. The element size needed to be reduced and the mesh had to be improved to keep the mesh metric factors within the limits allowed, which will reveal the network quality; else, the solution may include inaccuracy.

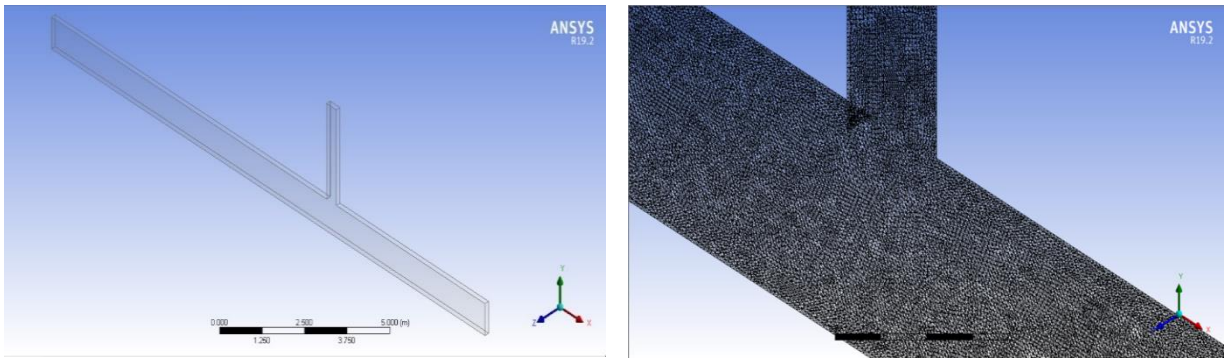

(a) (b)

Figure 6 A 3-D view of; (a) geometry, and (b) zoomed mesh elements.

The 'Grid Independence Test' (GIT) a well-known process, was employed to test several meshes and identify an optimum grid size for this study. Inaccurate results will stem from low numbers and grid elements that yield particles of coarse size; more analysis time will be consumed if a fine mesh is used. Therefore, the GIT ANSYS DesignModeler program, to provide accurate results, indicates a specific grid density that will be suitable if the simulation time is reduced. These findings are endorsed with experimental results, for accuracy. Once only a minor divergence from the prior works is achieved, the cases are considered acceptable.

20-mm mesh size is generated using tetrahedral items because the results of the verification implied greater accuracy for these elements rather than for the hexahedron ones (Table 2). The details of the grid generation are shown in Table 3. The mesh metric parameters (skewness, orthogonal quality, and aspect ratio) of the grid options adopted in this study were tested and compared with the permissible limit as identified in Table 4. Consequently, the rating of the mesh quality was in the range of Very good to Excellent. After creating the mesh, names are assigned to the boundary condition surfaces, after which their function, hydraulic characteristics, and operating settings, and are included in the setup process steps.

Table 1 Standard mesh metric parameters of ANSYS Fluent software [26-28].

Skewness	**Unacceptable**	**Bad**	**Acceptable**	**Good**	**Very good**	**Excellent**
	0.98-1	0.95-0.97	0.8-0.94	0.5-0.8	0.25-0.5	0-0.25
Aspect Ratio	The Aspect Ratio is a measurement of element quality, with 1 indicating a perfectly formed tetrahedral element and raising the Aspect Ratio indicating a degradation of the element shape.					
Orthogonal Quality	**Unacceptable**	**Bad**	**Acceptable**	**Good**	**Very good**	**Excellent**
	0-0.001	0.001-0.14	0.15-0.2	0.2-0.69	0.7-0.95	0.95-1

Table 2 The verification of mesh elements form for two sections located in the experimental test.

Elements form	**Cross-section at an axial distance of 11.43 m**			**Cross-section at an axial distance of 11.63 m**		
	MAE	**RMSE**	**MARE**	**MAE**	**RMSE**	**MARE**
Hexahedron	0.025273	0.033837	0.066983	0.025273	0.033385	0.072113
Tetrahedron	0.015455	0.022764	0.039283	0.0150	0.028324	0.042754

Annotation: RMSE indicates the root mean square error, MAE denotes the mean absolute error, and MARE signifies the mean absolute relative error.

Table 3 Mesh details of the present study.

Elements characteristics	
Element shape	Tetrahedron
Advanced options	Curvature and proximity capture
Element size	20 mm
Nodes	584835
Elements	3148581
Mesh metric parameters (average values)	
Skewness	0.21778
Aspect ratio	1.8328
Orthogonal quality	0.78081

*2.2.2.*Setup and solution

In FLUENT, the setup and solution solvers include recognition of the boundary conditions, setting the fluid characteristics, choosing the suitable logarithms, and arriving at the solution. Depending upon the type of practical experimental flow chosen, the precise field conditions need to be addressed. The Boundary Conditions (BCs) consider all the areas enclosing the model domain. Following the User Guide guidelines provided for modeling open-channel flows in the ANSYS FLUENT program, identification of the BCs was done [29]. The term velocity-inlet condition is applied to the inlet section of the upstream main channel. This BC assumes constant and uniform velocity distribution over the cross-section. Apart from the water surface and velocity magnitude, the turbulent intensity is another requirement for this BC, in which the condition of the velocity-inlet is used to compute the value of the velocity; this is accomplished through division of the discharge at the upstream inlet by the area of the cross-section of the main channel. The BC turbulence specification method is the ratio of the turbulence intensity to the viscosity. The outflow boundary conditions were set for two exits of the intake and main channels, for all the simulations. According to the flow properties in the laboratory experiments the quantities for both inflow and outflow BCs were ascertained and calculated, following the procedure recommended in FLUENT. The top surface of the geometry was defined as a condition of symmetry as the Froude number was less than 0.4, and a rigid lid could be used as a substitute for the water surface [30]. This BC warrants a free-surface condition, in which at the flow surface the value of the shear stress is zero [31]. Using the shear condition option of 'No Slip', the sidewalls and bed surfaces were chosen as the wall boundary conditions. The height of the roughness was more realistically adjusted to suit the wall boundary condition (wetted perimeter).

The ANSYS FLUENT program allows the user to choose from a selection of flow conditions and algorithms, as well as spatial discretization methods and many viscous models, to maximize the processing efficiency [24,29]. After performing the simulation for all the setup conditions mentioned above, covering the various sections of the experimental data selected for this study, these setup characteristics were recognized as having the highest accuracy and complied with the experimental findings. These setup characteristics that were adopted are summarized in Table 4. The error proportions for a variety of viscous models, at two sections, are listed in Table 5. As displayed in Figure 7, these values are also compared. Based on the results of the validation, the numerical model is the one that most closely matched the experimental model.

Table 4 Setup parameters.

Solver's conditions and algorithms	**Type**
General conditions	
Solver type	Pressure- Based
Time	Transient
Viscous model	
k-ω model	SST
Options	Curvature correction
	Production limiter
Solution method	
Transient Formulation	First Order Upwind
Pressure-Velocity Coupling	
Scheme	SIMPLEC
Spatial discretization method	
Gradient	Least Squares Cell Based

Volume fraction	Compressive
Pressure	PRESTO
Momentum	First Order Upwind
Turbulence kinetic energy	First Order Upwind
Specific dissipation rate	Second Order Upwind

Table 5 Validation of the viscous models with error percent for two sections of the laboratory data at a diversion ratio of 16%.

Viscous model	Cross-section at an axial distance of 11.43 m			Cross-section at an axial distance of 11.63 m		
	MAE	RMSE	MARE	MAE	RMSE	MARE
[SST] k-ω	0.01545	0.02276	0.03928	0.015	0.02832	0.04275
Standard & [RNG]k-ε	0.01890	0.02660	0.04847	0.01718	0.02991	0.04937
RSM	0.01972	0.0270	0.05083	0.01709	0.02986	0.04861

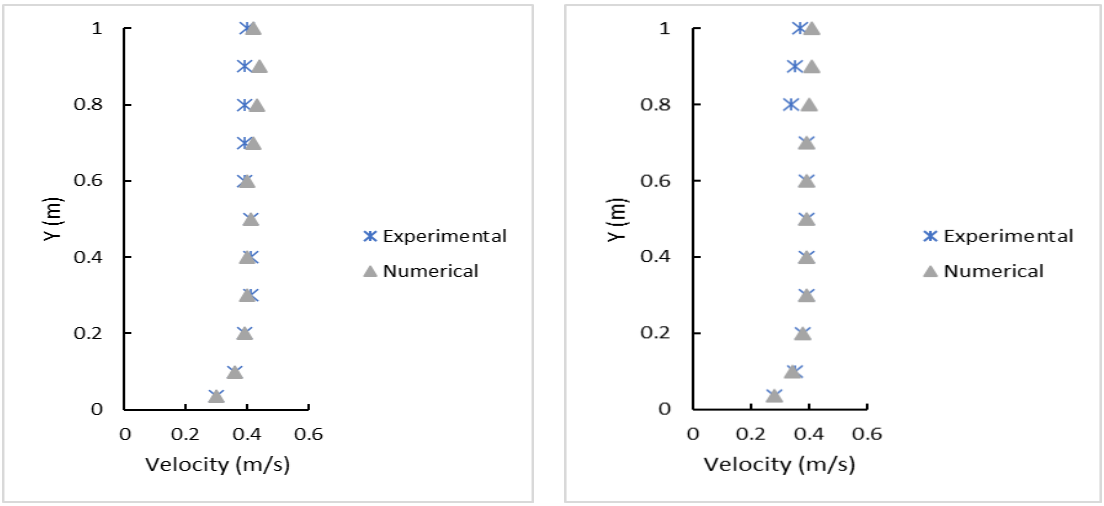

Figure 7 Illustration of velocity distribution obtained from the current numerical simulation and the laboratory test conducted by Omidbeigi et al. [25] at z = 0.09 m and a discharge ratio of 16% at two intake cross-sections. (a) x = 11.43 m. (b) x=11.63 m.

3. DESCRIPTION OF MODELS

In this study, the flow characteristics at a lateral diversion are simulated in two ways. In the first scenario, the effect of the discharge ratio Qr,(intake outlet discharge divided by the upstream main channel discharge), on the size of the separation vortex, is described. Five models had simulated different discharge ratios (16%, 20%, 30%, 40% and 50 %). Table 6 and Figure 8 reveal the hydraulic conditions and zoomed intake connection geometry utilized in this scenario, respectively. The second scenario investigates the effects of making changes to the geometric features of the intake entrance shape. In this scenario, different designs of the geometry of the intake inlet are modeled to decrease the separation zone size, as well as to ensure that the bed shear stress is redistributed across the intake port. These configurations have been considered and developed based on the suggested models of Helal [19]; who examined the effects of three confluence junction shapes (sharp, chamfered, and rounded downstream edge). Model A is distinguished by the chamfered inner corner angle of 30° to the flow direction. In Model B, however, the intake entrance has a chamfered outer edge at a 30° angle with the horizontal. In fact, in Figures 9, 10, and 11 the models of A, B, and C, respectively, are shown. More details are provided for the simulation cases of each model in Table 7. For all cases in the second scenario, 0.16 was the discharge ratio chosen for the preparation of a clearer separation zone. It must be noted that the term “Original Case” indicates a state-employed during the validation which possesses the identical geometry, Boundary Conditions, and flow features utilized in the experimental setup test.

Table 6 The simulated domain's hydraulic variables.

Inlet discharge(Q) (lit/s)	Flow Depth(d_o) (m)	Average inlet velocity (U_0) (m/s)	Fr	Discharge ratio (Qr)=(Q_2/Q)	Q_1(lit/s)	Q_2(lit/s)
58	0.15	0.38	0.31	16%	9.28	48.72
				21%	12.18	45.82
				30%	17.4	40.6
				40%	23.2	34.8
				50%	29	29

Where: Fr indicates Froude number, Q is inlet discharge (m^3/s), Q_1 is outlet discharge from the main channel (m^3/s), Q_2 is outlet discharge from the branch channel (m^3/s), and the discharge ratio, Qr= (Q_2/Q).

Table 7 The cases of the simulation designs.

Simulation type		The Special scenarios of the models
Various discharge ratios (Qr)	1	Qr=16%
	2	Qr=21%
	3	Qr=30%
	4	Qr=40%
	5	Qr=50%
Model A Chamfered outer corner at α=30°	1	c=0.25 b
	2	c=0.5 b
	3	c=0.75 b
	4	c= b
Model B Chamfered inner corner at α=30°	1	c=0.25 b
	2	c=0.5 b
	3	c=0.75 b
	4	c= b
Model C Chamfered and rounded inner corner at α=30°	1	c=0.25 b
	2	c=0.5 b
	3	c=0.75 b
	4	c= b

The simulations listed above are all established on the same basic simulation steps of the method of validation, incorporating a simple alteration in the geometry discharge ratio. In two scenarios, at two intake cross-sections located at 1.15m (Section 1) and 1.5m (Section 2) in the y-direction, the shear stress of the bed surface of the intake is investigated. In addition to the path lines with velocity contours at 0.04 m height above the bed surface, and the separation zone dimensions of width and length. The width (Ws) and length (Ls) of the separation region were normalized by, respectively, the width and length (Wi and Ls) of the lateral channel. In ImageJ program, separation vortex length and width were computed. Figures 12 reveal the measurements of the separation zone. The Cartesian coordinate system, as appointed in Figure 13, covers all the coordinates cited in this study.

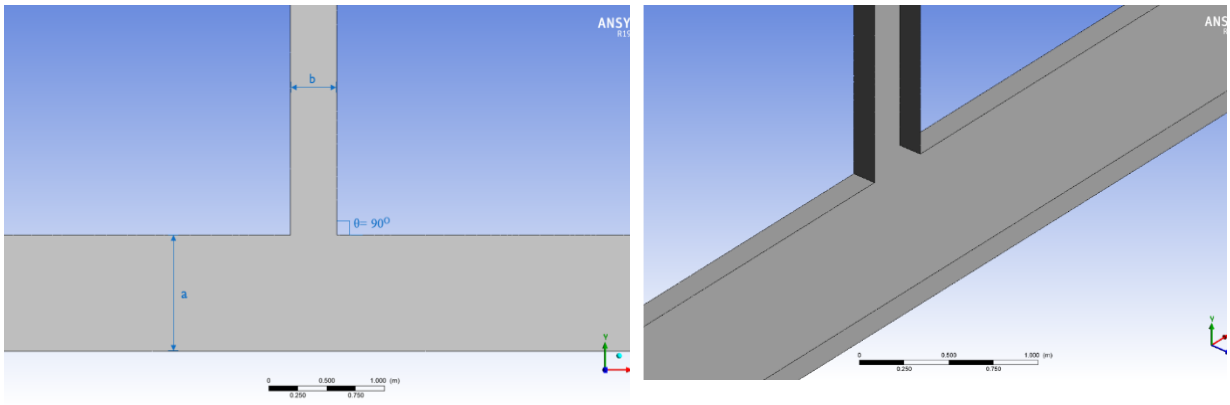

Figure 8 Three-dimensional and schematic plan of the lateral intake entrance of the original case.

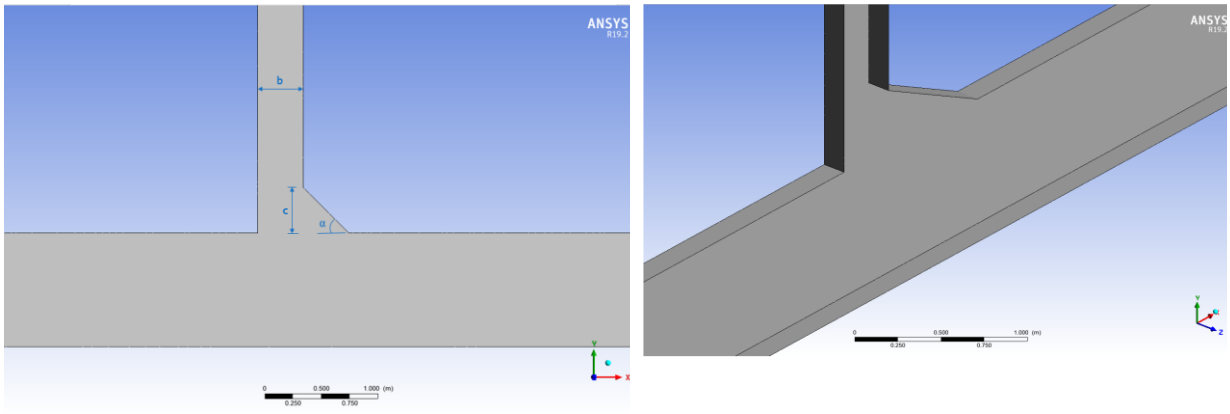

Figure 9 Plan and 3-D geometric model of the chamfered outer edge of the intake entrance.

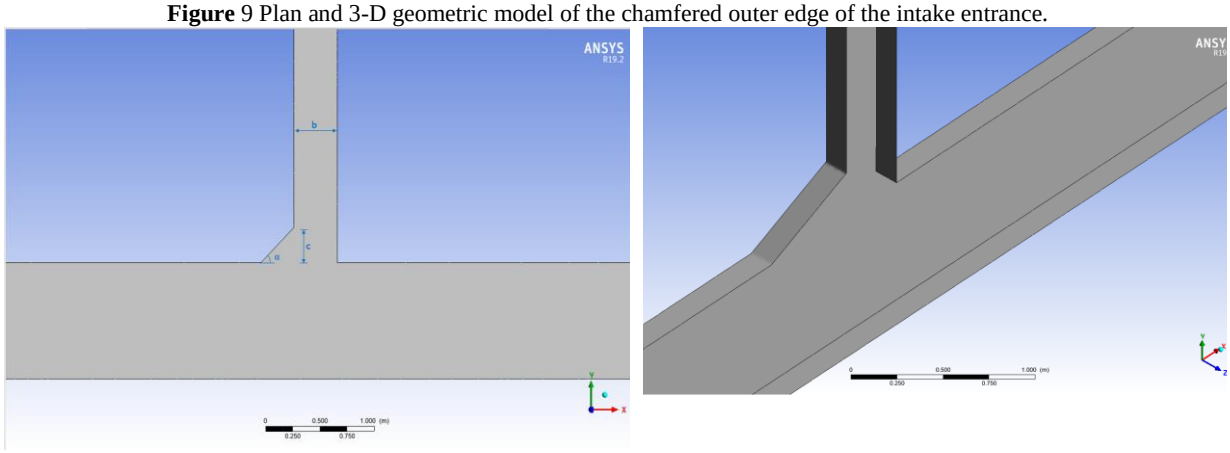

Figure 10 Model B, chamfered inner corner case.

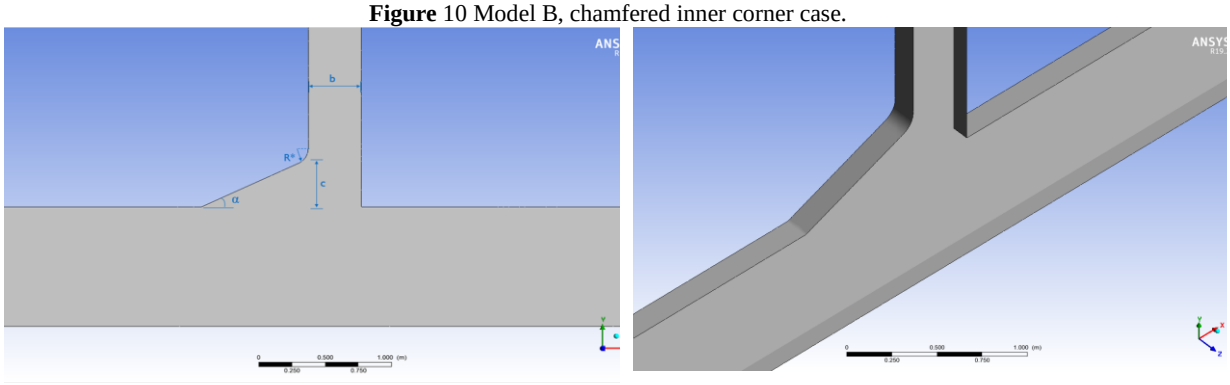

Figure 11 The chamfered and rounded inner corner view, Model C.

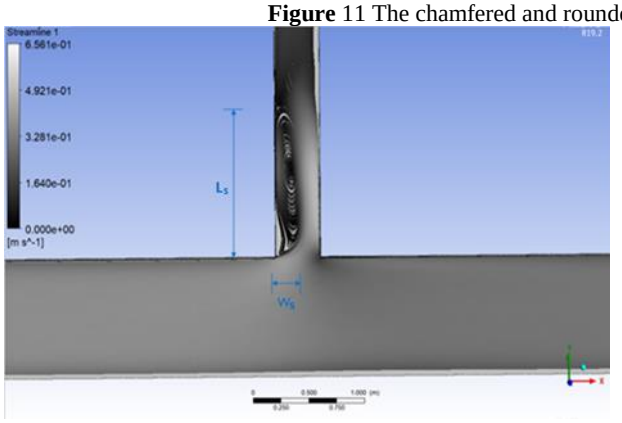

Figure 12 Plan depicts the separation area dimensions.

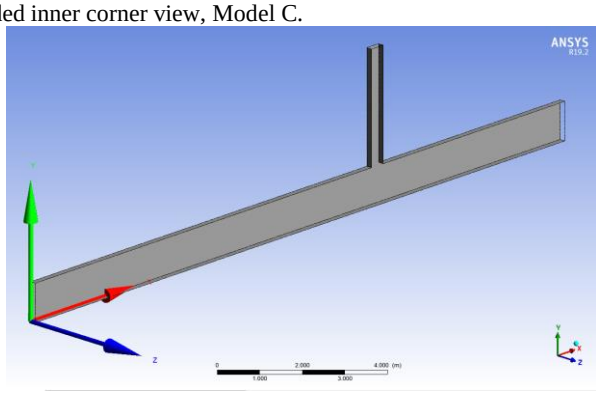

Figure 13 Cartesian origin point position**.**

4. RESULTS AND DISCUSSION

4.1. Various discharge ratio results

By comparing the different discharge ratios cases, Figure 14 (a-e), it was observed that separation zone width and length are decreased with the increase of Qr percent. This matches the results of previous studies conducted by Pizardeh & Shamloo [3], Ramamurthy et al. [8], Neary et al, [9], Rezapour et al [20], and Omidbeigi et al. [25]. These measurements are also explained in Figures 4a and 4b. When the discharge ratio is increased from 0.16 to 0.50, flow velocity increases, and flow passes faster of the opposite bank of the intake. Therefore, the region with higher velocities is displaced nearer the side intake entry, causing the sediment portions to enter the side intake. However, when the width of the separation area narrows, the vortex's ability to extract sediments declines, resulting in less sedimentation in this area.

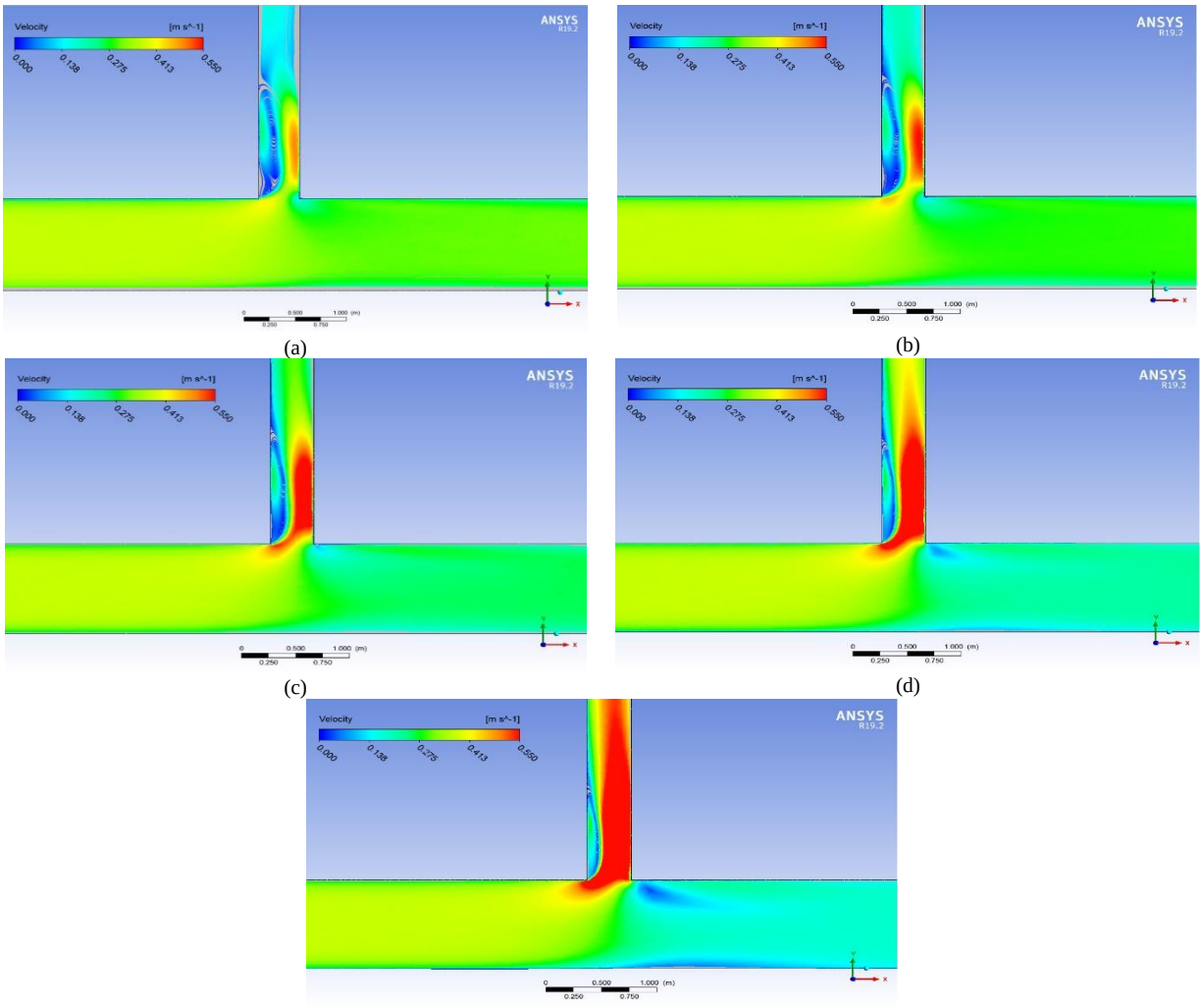

Figure 14 Streamlines with velocity contours shows the separation zone at various discharge ratios, (a) Qr=0.16, (b) Qr =0.21, (c) Qr =0.3, (d) Qr =0.4, and (e) Qr =0.5.

Also, due to the high velocity and rotation of secondary flows, erosion occurs within the channel in the flow region [32]. Figure 15 depicts the increase in shear stress with a higher discharge ratio. As a result, as the discharge ratio rises, the intake port area on the opposite bank becomes more eroded, while the separation area becomes less susceptible to sedimentation (Figures 15 &16).

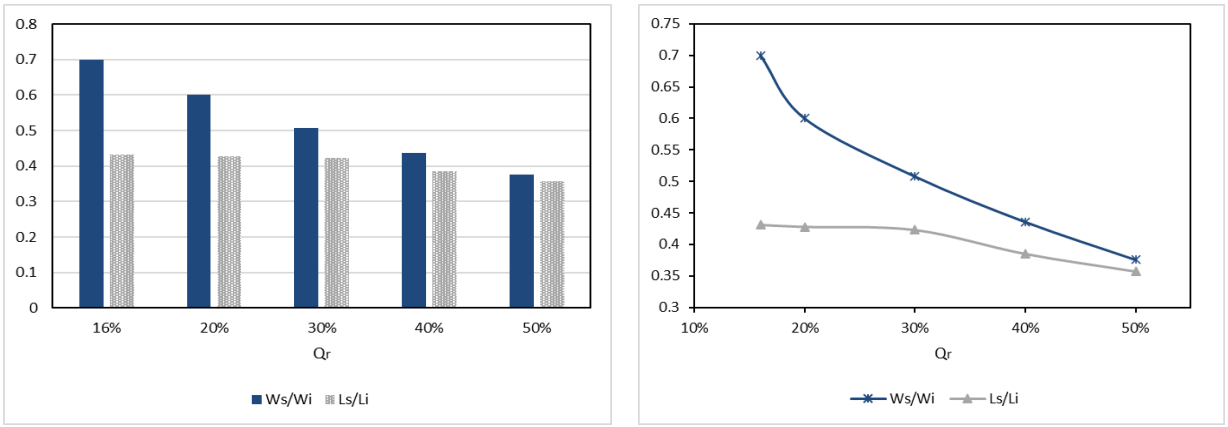

Figure 15 Separation region dimensions for different discharge ratios of the original model geometry.

The low shear stress zone is associated with the separation zone, according to the shear stress contours in Figure 16. By comparing Figures 16 (a to e) it is seen that since the discharge ratio rises from 0.16 to 0.5, the flow has a high momentum towards the downstream main flow. Thus, the dividing stream surface extends out into the main channel as the discharge ratio decreases resulting in increasing the low-stress zone. Additionally, increasing the discharge ratio causes growing and extending the high shear stress region due to increasing the velocity and secondary flow strength as displayed in Figure 17. However, when the discharge ratio (Qr) increases, the quantity of influx deviates more towards the intake mouth, increasing the rate of sediment entry transported carried with the flow discharge into the intake [33].

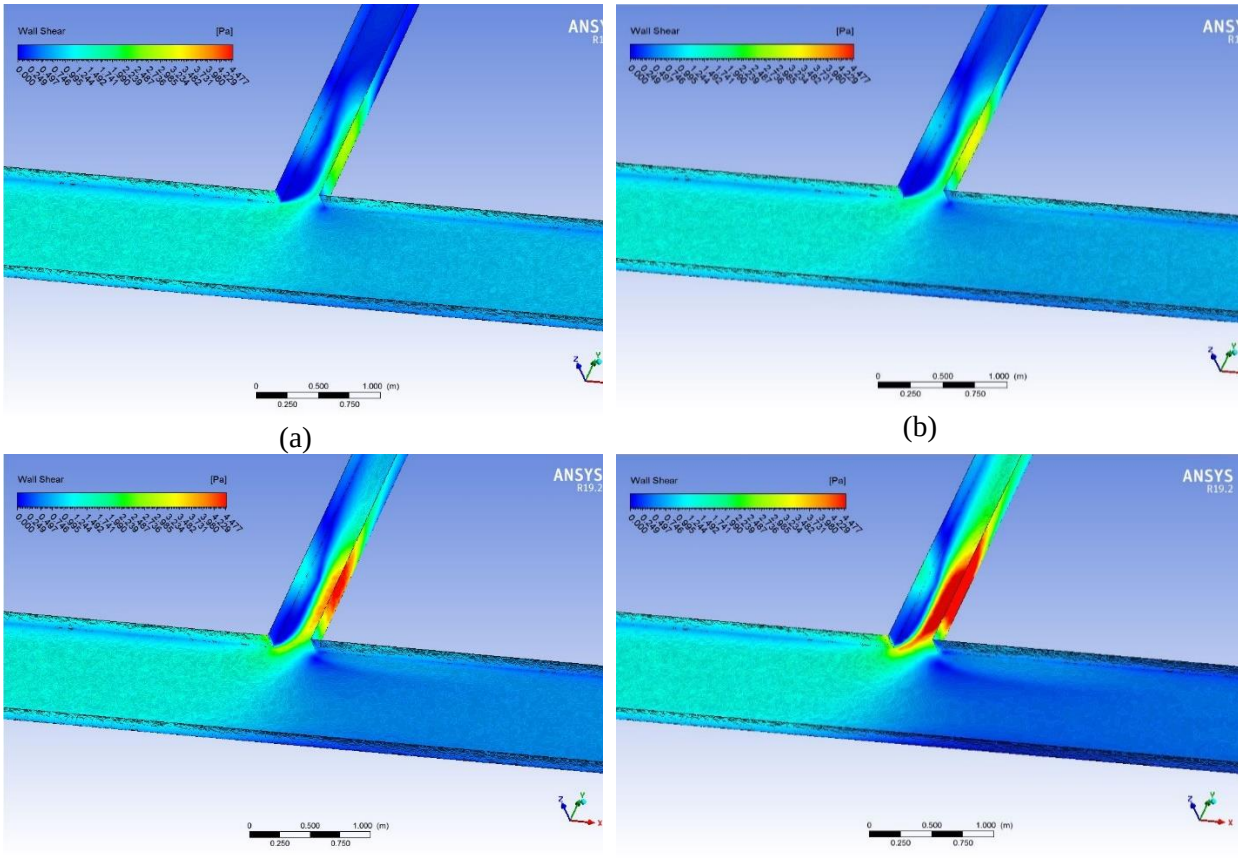

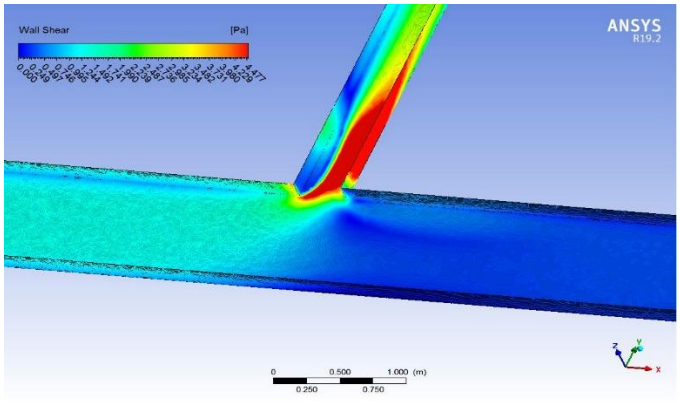

(e)

Figure 16 Wall shear stress values for different discharge ratios at the lateral intake channel. (a)Qr=16%, (b) Qr=20%, (c) Qr=30%, (d) Qr=40%, and (e) Qr=50%.

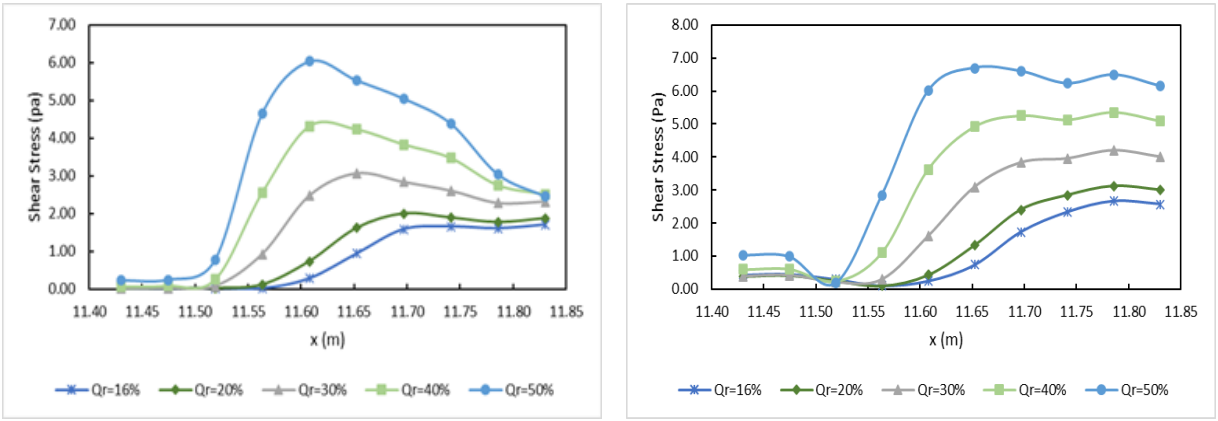

Section 1 Section 2

Figure 17 Bed shear for numerous discharge ratios at two intake cross-sections.

4.2. Changing the geometry of the intake junction

For the cases of the intake inlet with the external chamfered angle, the velocity contours and separation zone dimensions are shown in Figures 18 and 21-a, respectively. For this case, all the simulation results revealed the negative effect it exerted on the flow pattern, due to many causes. First, in all the cases, the flow separation zone showed an increase along the inner wall. Second, in response to an increase in the size of the cuttings, a new spiral is seen to emerge and this, in turn, intensifies the problems. However, while cutting the inner corner of the intake channel inlet, the size of the region was considerably underestimated, as shown in Figures 19 and 21-b. Here the ratios of the separation area width and length have been decreased to 82% and 50 %, respectively. Further, as is obvious in Figures 20 and 21-c, when the internal corner of the side-intake inlet was cut, the chamfered and rounded edge (Model C), revealed that the ratio of the separation region width and length had decreased to 90% and 72 %, respectively.

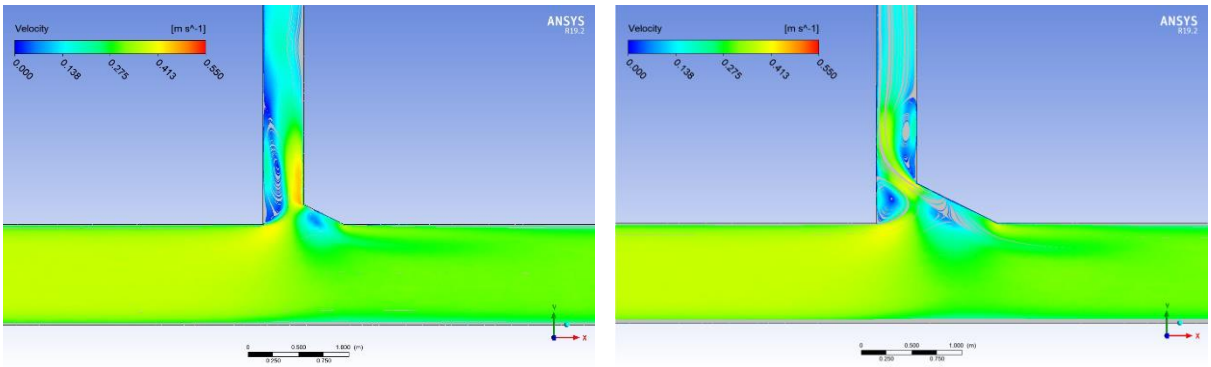

c=0.5 b c= b

Figure 18 Chamfered outer edge configuration with α=30°, model A.

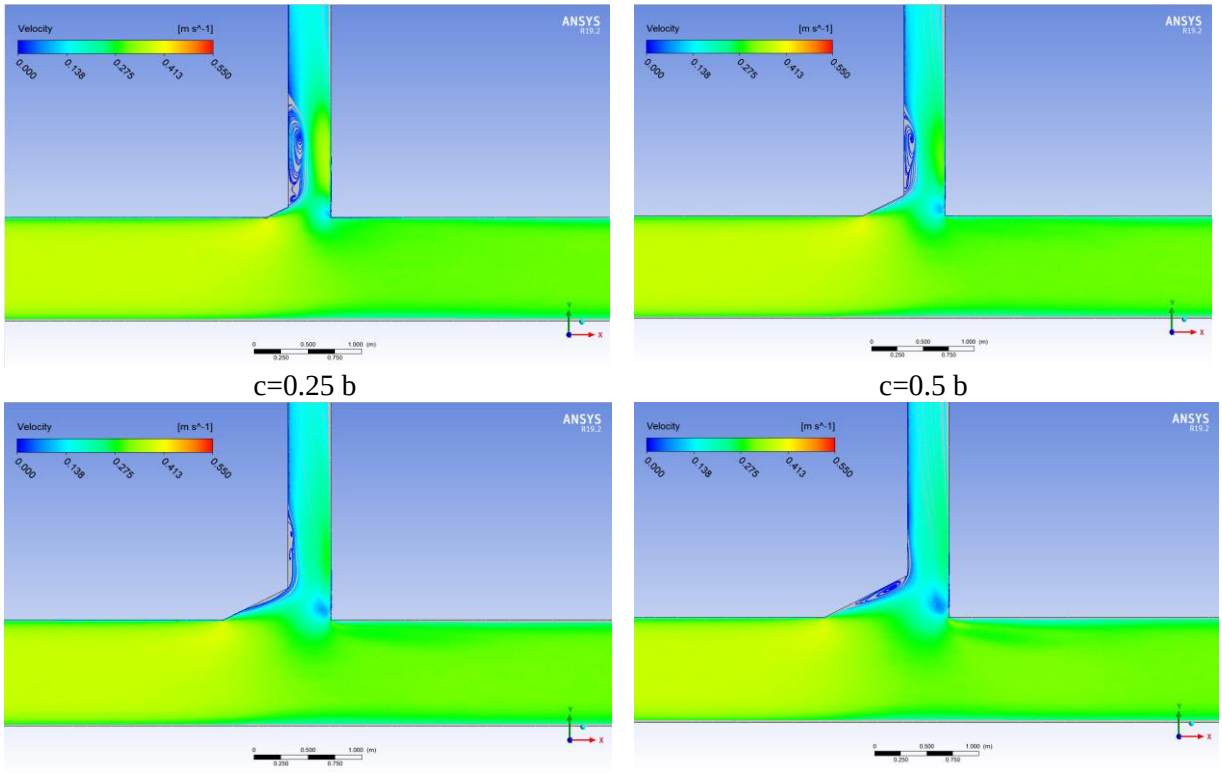

c=0.25 b c=0.5 b

c=0.75 b c= b

Figure 19 Model B represented by the chamfered internal edge of the intake junction for several values of the chamfer length (c) at α=30º.

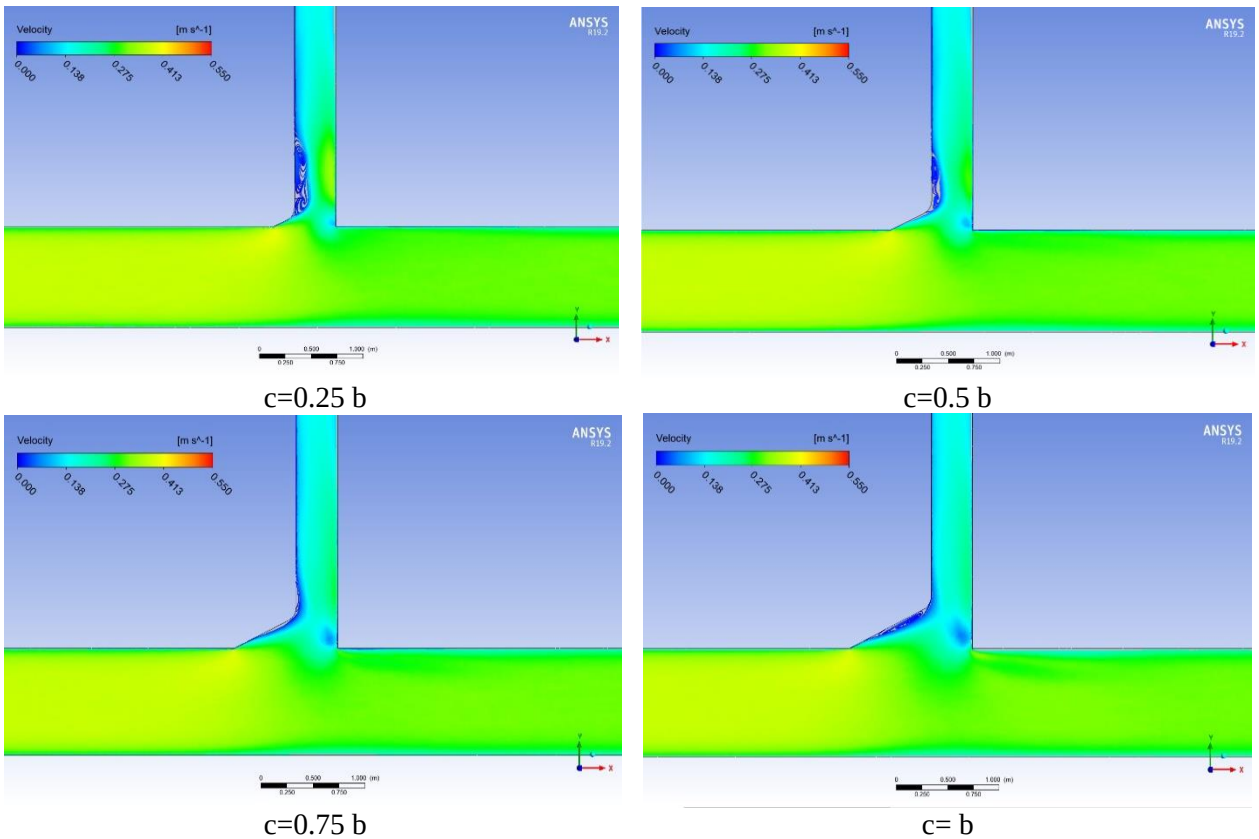

c=0.25 b c=0.5 b

c=0.75 b c= b

Figure 20 degree rounded and chamfered inner corner (Model C)

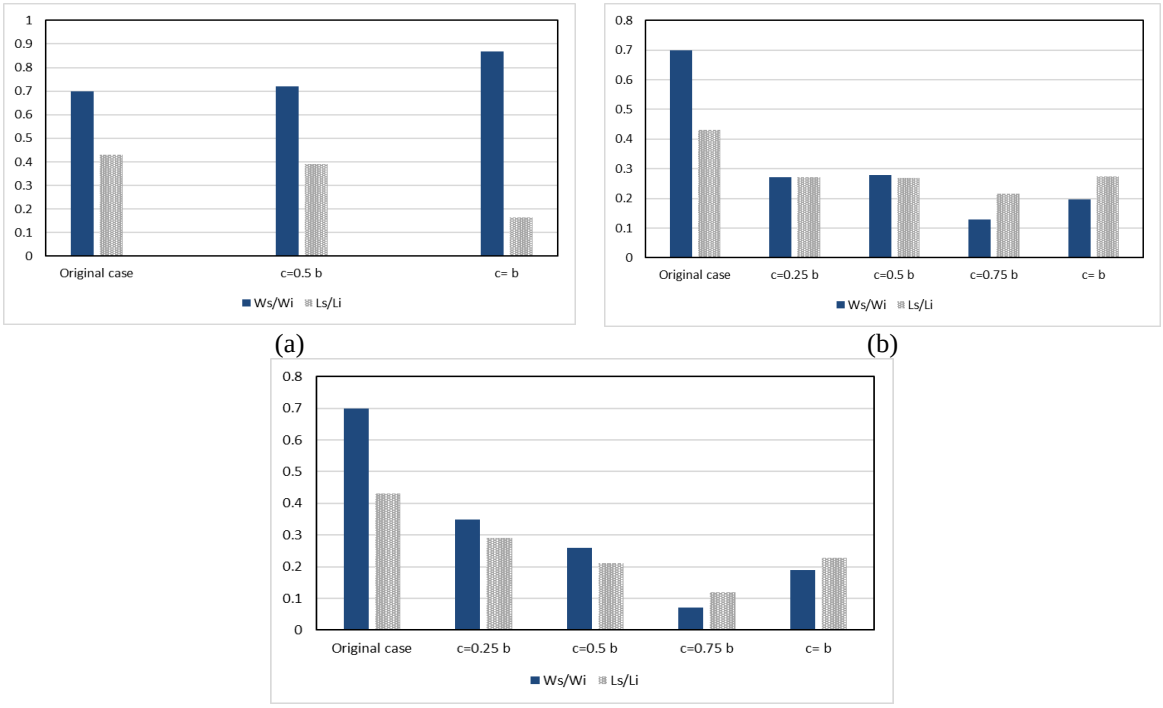

Figure 21 Separation zone dimension for models of; (a) Chamfered outer corner of the diversion channel inlet at α=30° (Model A), (b) Chamfered inner corner of the diversion intersection at α=30° (Model B), and (c) rounded and chamfered inner corner at α=30° (Model C).

Figure 22 represents the bed shear at the two sections located at the intake entrance, Section 1 and Section 2, for the chamfered inner cases (Model B cases) as well as the original case model. In the circumstance of a non-chamfered intake edge (Original Case), substantially greater shear stress is seen at the two sections downstream (or the opposite bank) of the intake port, which reduces as it inclines towards the beginning of the intake. Hence, the internal intake bank may be subject to sediment deposition, unlike the remote bank, which shows a tendency for erosion. However, when the inner corner of the intake is changed from a 90° sharp edge to a chamfer shape at 30° with horizontal, the shear stress becomes practically consistent across the width of the intake. Corresponding to the lowest shear stress pattern of the original case, the shear stress for the chamfered inner corner models displays higher values. However, the bed shear stress downstream side of the intake for the original case is markedly greater than the other modified inner corner models (Model B), as depicted in Figure 22. From these findings, it was clear that by raising the shear stress upstream the diversion junction and lowering it at the end of the intake entrance, the problems of scouring and sedimentation are reduced in sections of the intake inlets as seen in Figure 22.

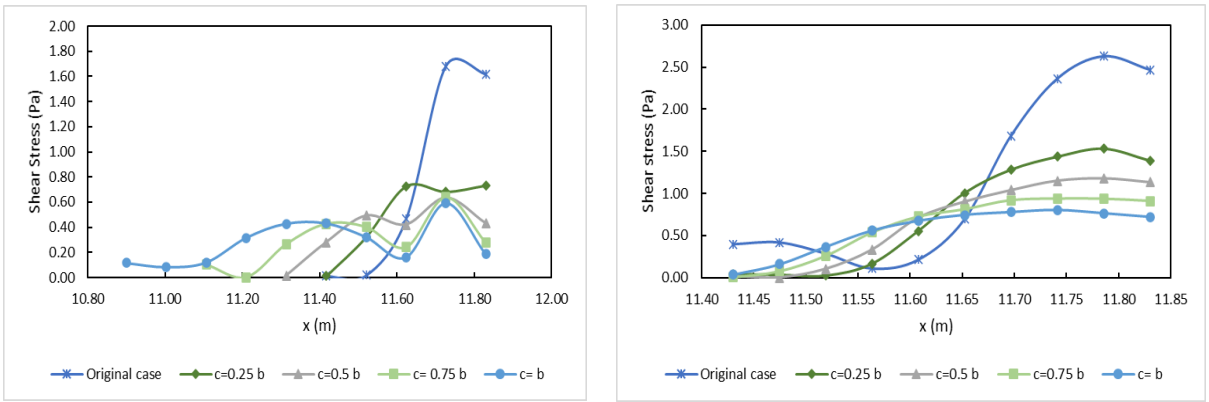

Section 1 Section 2

Figure 22 Bed shear stress measurements for varied values of c at α=30° for the models of the chamfered inner edge of the intake entry.

5. CONCLUSIONS

In the present research, simulations were performed using ANSYS FLUENT program to investigate the effects of various hydraulic and geometrical characteristics on flow and sediment patterns at the lateral intake. For this purpose, velocity and bed shear stress values were calculated that are as indicators of sedimentation and erosion. In addition, separation region dimensions were measured to predict the sedimentation potential. Five discharge ratios were examined. Then, three intake inlet modifications were numerically studied. Results indicate that increasing the flow diversion ratio, from 16% to 50%, shortens the separation zone dimensions. In addition, as the discharge ratio escalated, greater erosion was observed in the region of the intake port area on the opposite bank, and correspondingly, the separation zone showed lower susceptibility to sedimentation, in terms of the values of the bed shear stress. On the other hand, adjusting the 90º diversion channel can enhance the flow pattern and redistribute bed shear stress at the diversion junction. Sedimentation and erosion concerns are reduced as a result. It was also realized that in several situations, altering the diversion upstream corner had a negative impact. The following aspects were discovered as a result of diversion geometry modeling:

1. The chamfered opposite edge of the intake junction, the outer corner downstream intake inlet (Model A), particularly the larger size of the chamfer, has undesirable impacts on the separation zone and velocity distribution. This results in strengthening the separation eddy, thus trapping more sediment in this zone.

2. The best model capable of reducing the separation zone was found to be the intake geometry having a chamfered and rounded inner edge with a 30º angle to the direction of flow (Model C) and a chamfer dimension that parallel the intake flow direction (c distance) of the three-quarters of the intake width. For this scenario, the width and length of the separation zone are reduced to 90% and 72 %, respectively.

Finally, modifying the diversion junction geometry requires precision and caution based on the findings of this study.

REFERENCES

1. Goudarzizadeh, R., Hedayat, N., & Jahromi, S. M. (2010). Three-dimensional simulation of flow pattern at the lateral intake in straight path, using finite-volume method. *World Academy of Science, Engineering and Technology*, 47, 656-661.
2. Firozjaei, M. R., Neyshabouri, S. S., Sola, S. A., & Mohajeri, S. H. (2019). Numerical simulation on the performance improvement of a lateral intake using submerged vanes. *Iranian Journal of Science and Technology, Transactions of Civil Engineering*, 43(2), 167-177.
3. Shamloo, H., & Pirzadeh, B. (2008). Investigation of characteristics of separation zones in T-junctions. *WSEAS transactions on Mathematics*, 7(5), 303-312.
4. Mohammadiun, S., Neyshabouri, S. S., Naser, G., & Vahabi, H. (2016). Numerical investigation of submerged vane effects on flow pattern in a 90 junction of straight and bend open channels. Iranian Journal of Science and Technology, *Transactions of Civil Engineering*, 40(4), 349-365.
5. Bowles, C. (1999). An investigation into the flow structure of a generalised open channel intake. Nottingham Trent University (United Kingdom).
6. Marra, W. A., Parsons, D. R., Kleinhans, M. G., Keevil, G. M., & Thomas, R. E. (2014). Near-bed and surface flow division patterns in experimental river bifurcations. *Water Resources Research*, 50(2), 1506-1530.
7. Dutta, S., Fischer, P., & Garcia, M. H. (2016). Large eddy simulation (LES) of flow and bedload transport at an idealized 90-degree diversion: Insight into Bulle effect. River Flow 2016: Iowa City, USA, July 11-14, 2016, 101.
8. Ramamurthy, A. S., Qu, J., & Vo, D. (2007). Numerical and experimental study of dividing open-channel flows. *Journal of Hydraulic Engineering*, 133(10), 1135-1144.

9. Neary, V. S., Sotiropoulos, F., & Odgaard, A. J. (1999). Three-dimensional numerical model of lateral-intake inflows. *Journal of Hydraulic Engineering*, 125(2), 126-140.
10. Bulle, H. 1926. Untersuchungen uber die Geschiebeableitung bei der Spaltung von Wasserlaufen. VDI Verlag, Berlin (in German).
11. Herrero, A., Bateman, A., & Medina, V. (2015). Water flow and sediment transport in a 90 channel diversion: an experimental study. *Journal of Hydraulic Research*, 53(2), 253-263.
12. Odgaard, A. J. (2009). River training and sediment management with submerged vanes. Virginia, US: ASCE Press.
13. Odgaard, A. J., & Wang, Y. (1991). Sediment management with submerged vanes. I: Theory. *Journal of Hydraulic Engineering*, 117, 267–283.
14. Odgaard, A. J., & Wang, Y. (1991). Sediment management with submerged vanes. II: Applications. *Journal of Hydraulic Engineering*, 117, 284–302.
15. Barkdoll, B. D., Hagen, B. L., & Odgaard, A. J. (1998). Experimental comparison of dividing open-channel with duct flow in T-junction. *Journal of Hydraulic Engineering*, 124(1), 92-95
16. Omidbeigi, M. A., Ayyoubzadeh, S. A., & Safarzadeh, A. (2009, August). Experimental and numerical investigations of velocity field and bed shear stresses in a channel with lateral intake. *In 33rd IAHR Congress*, Vancouver, Canada (pp. 1284-1291).
17. Fan, Y. A. N. G. (2008). Study on diversion angle effect on lateral intake flow [J]. *Journal of China Institute of Water Resources and Hydropower Research*, 1.
18. Karami Moghadam, M., Amini, A., & Keshavarzi, A. (2020). Intake design attributes and submerged vanes effects on sedimentation and shear stress. *Water and Environment Journal*, 34(3), 374-380.
19. Helal, Esam E. Y., (2006). "Improving the Flow Characteristics at Open Channel's Junctions", Ph.D. Thesis, Dept. of Civil Engineering, El-Minufiya University, Egypt.
20. Rezapour, S., Moghadam, K. F., & Omid Naceni, S. T. (2009, August). Experimental study of flow and sedimentation at 90◦ open channel diversion. In *Proceedings of the 33rd IAHR Congress*, Vancouver, BC, Canada (pp. 9-14).
21. Ramamurthy, A. S., Minh Tran, D., & Carballada, L. B. (1990). Dividing flow in open channels. *Journal of Hydraulic Engineering*, 116(3), 449-455.Ramamurthy, A. S., Minh Tran, D., & Carballada, L. B. (1990). Dividing flow in open channels. *Journal of Hydraulic Engineering*, 116(3), 449-455.
22. Lama, S. K., Kuroki, M., & Hasegawa, K. (2002). Study of flow bifurcation at tic 30° open channel junction when the width ratio of branch channel to main channel is large. *PROCEEDINGS OF HYDRAULIC ENGINEERING*, 46, 583-588.
23. Schiano, P. (1996). CS Ierotheoul, CR Forsey', MLeatham', U Block. Parallel Computational Fluid Dynamics' 96: *Algorithms and Results Using Advanced Computers*, 197.
24. Fluent, U. S. G. (2003). Fluent inc. Chapter, 6, 14-6.
25. Omidbeigi, M. A., Ayyoubzadeh, S. A., & Safarzadeh Gendeshmin, A. (2012). Experimental and numerical study of three dimensional flow structure at lateral intake. *Modares Civil Engineering journal*, 12(1), 0-0.
26. Ozen, M., & Fellow, A. S. M. E. (2014, November). Meshing workshop. In MESHING WORKSHOP (p. 25).

27. Noor, M. M., Wandel, A. P., & Yusaf, T. (2013, July). Detail guide for CFD on the simulation of biogas combustion in bluff-body mild burner. *In Proceedings of the 2nd International Conference of Mechanical Engineering Research (ICMER 2013)* (pp. 1-25). Universiti Malaysia Pahang.
28. Airfoil, N. (2010). ANSYS FLUENT.
29. ANSYS, A. L. D. (2017). user guide, ANSYS. Inc. version, 15.
30. Taylor, E., "Flow characteristics at rectangular open channel junction," *Journal of Hydraulic Engineering*, ASCE, 10 (6).893- 902. Jun. 1944.
31. Barkdoll, B. D., Hagen, B. L., & Odgaard, A. J. (1998). Experimental comparison of dividing open-channel with duct flow in T-junction. *Journal of Hydraulic Engineering*, 124(1), 92-95
32. Karami, H., Farzin, S., Sadrabadi, M. T., & Moazeni, H. (2017). Simulation of flow pattern at rectangular lateral intake with different dike and submerged vane scenarios. *Water Science and Engineering*, 10(3), 246-255.
33. Habibi, H., Masjedi, A., Pourmohammadi, M. H., Kamanbedast, A. A., & Bordbar, A. (2017). Reduction of sediment transport due to flood and runoff to a lateral intake in the river bend using submerged vane. *FEB-Fresenius Environmental Bulletin*, 6996.